H. Jiang

B. Liu

Y. Huang

Department of Mechanical and Industrial Engineering,
University of Illinois,
Urbana, IL 61801

K. C. Hwang

Department of Engineering Mechanics,
Tsinghua University,
Beijing, China 100084

Thermal Expansion of Single Wall Carbon Nanotubes

We have developed an analytical method to determine the coefficient of thermal expansion (CTE) for single wall carbon nanotubes (CNTs). We have found that all CTEs are negative at low and room temperature and become positive at high temperature. As the CNT diameter decreases, the range of negative CTE shrinks. The CTE in radial direction of the CNT is less than that in the axial direction for armchair CNTs, but the opposite holds for zigzag CNTs. The radial CTE is independent of the CNT helicity, while the axial CTE shows a strong helicity dependence. [DOI: 10.1115/1.1752925]

1 Introduction

Due to their superior material properties, carbon nanotubes (CNTs) [1] have many potential applications such as nanoscale sensors, nanocomposites, and nanoelectronics (e.g., [2–6]). Some examples of nanoelectronics include the next-generation computers (e.g., [7]) and nanotube transistors [8–15]. These CNT-based nanoelectronic devices may experience high temperature during manufacture and operation. This leads to thermal expansion and residual stress in devices, and affects the device reliability. Therefore, the coefficient of thermal expansion (CTE) of CNTs is an important property for CNT-based nanoelectronics. This is similar to Si, which is the dominant micro-electronic material today. The CTE of Si has been thoroughly investigated in the last few decades (e.g., [16–25]). The CTE of Si displays an unusual and intriguing temperature dependence, namely being negative (i.e., thermal contraction) at low temperature, and positive (i.e., thermal expansion) at high temperature (e.g., [21,23]).

The studies on the CTE of CNTs, however, are very limited due to the challenge in nanoscale experiments and modeling. There are very few experimental studies on the CTEs of multiwall CNTs [26,27] and CNT bundles [28,29]. Using the X-ray diffraction, Bandow [26] found that the CTE in the radial direction of multiwall CNTs is almost the same as the *c*-axis CTE of graphite. Yosida [28] and Maniwa et al. [29] also used the X-ray diffraction to study the CTEs of single wall CNTs bundles and their results suggest that the CNT bundles have negative CTE (thermal contraction) at low temperature and positive CTE (thermal expansion) at high temperature, similar to that of Si. Even though the CTE of single wall CNTs is important both to nanoelectronics and to the fundamental understanding of thermal properties of CNT bundles and CNT-polyethylene composites [30], there exists no experimental study on the CTE of single wall CNTs.

To the best of our knowledge, there exists only one molecular dynamics (MD) study on the CTE of single wall CNTs [31]. Based on the interatomic potential for carbon [32,33], Raravikar et al. [31] investigated the CTE of (5,5) and (10,10) armchair CNTs. The CTE in the radial direction of the CNT was found to be less than that in the axial direction. However, they reported only a single value for the CTE in the radial direction (also a single value for the axial CTE), and did not report any temperature dependence. This is contrary to the experiments of Yosida [28] and Maniwa et al. [29] which showed strong temperature dependence of CTEs for CNT bundles. Furthermore, the CTE of graphite, which can be considered as the CNT with infinitely large diameter, also has a strong temperature dependence, being negative at low and room temperature and positive at high temperature [34]. Therefore, the CTE of CNTs is anticipated to display strong temperature dependence.

This paper aims at a systematic study of the CTEs of CNTs, including their temperature dependence and the effect of CNT charality. Instead of using MD, which is computationally intensive and can simulate only up to nanosecond (10^{-9} s), we develop an analytic method to determine the CTE of CNTs directly from the interatomic potential [33] and the local harmonic model (e.g., [35]). This analytic method provides a simple and straightforward way to investigate the temperature and helicity dependence of the CTE of CNTs. Our results show that, similar to graphite, the CTE of CNTs is negative at low and room temperature, but becomes positive at high temperature. The range of negative CTE shrinks as the CNT diameter decreases. For armchair CNTs, we have confirmed Raravikar et al.'s [31] MD simulation results that the radial CTE is less than the axial one. However, for zigzag CNTs which were not studied by Raravikar et al. [31], we have found that the opposite holds, i.e., the radial CTE is larger than the axial one for zigzag CNTs. Furthermore, the radial CTE is found to be independent of the CNT helicity, but the axial CTE displays a strong dependence on the helicity.

The paper is outlined in the following. The atomic structure of the single wall CNT is shown in section 2. A set of finite (5) variables are introduced to quantitatively characterize this atomic structure. The CNT diameter, and the bond lengths and angles in the tubular structure of the CNT are all given in terms of these five variables. To account for the temperature effect, the Helmholtz free energy together with the local harmonic model are introduced in section 3 to determine these five variables at finite temperature. The equilibrium bond lengths and the coefficients of thermal expansion of the CNT are then obtained at each temperature. The coefficients of thermal expansion in the radial and axial directions of the CNT are given for armchair and zigzag single wall CNTs, and their dependence on temperature and CNT helicity are discussed.

2 Single Wall Carbon Nanotubes

2.1 Geometrical Representation of the CNT Structure. Figure 1(a) shows a schematic diagram of a CNT with the diameter d_t. Unlike a planar graphene sheet, a carbon atom and its three nearest-neighbor atoms on the CNT are not on a plane but form a tetrahedron because of the curvature effect. Depending on the bond orientation and the diameter of the CNT, carbon bonds on the CNT may have different lengths, and the bond angles deviate from 120 deg. Since a CNT can be considered as a rolled

Contributed by the Materials Division for publication in the JOURNAL OF ENGINEERING MATERIALS AND TECHNOLOGY. Manuscript received by the Materials Division December 15, 2002; revision received March 1, 2004. Associate Editor: H. Sehitoglu.

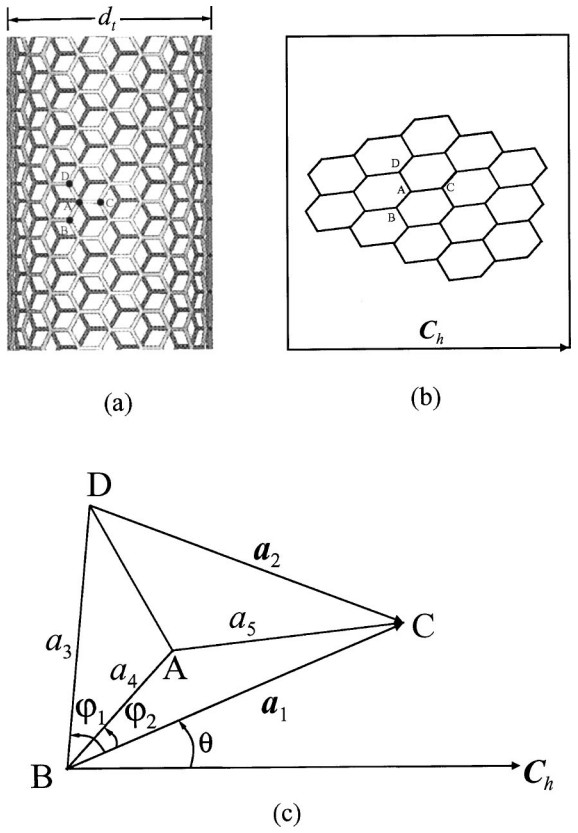

Fig. 1 A carbon nanotube (CNT): (*a*) the tubular structure of CNT; (*b*) a planar, "unrolled" CNT; and (*c*) a representative atom (A) and its three nearest-neighbor atoms (B, C, and D)

graphene sheet, we map the CNT shown in Fig. 1(a) to a two-dimensional, planar sheet of carbon atoms shown in Fig. 1(b). This mapping can be visualized by a cut of the CNT along its axial direction followed by the "unrolling" of the CNT to a plane without stretching. The distance between each pair of carbon atoms in the "unrolled" plane (Fig. 1(b)) is identical to the corresponding arc length on the CNT (Fig. 1(a)). It is important to point out that Fig. 1(b) is different from a graphene sheet since the bond lengths may not equal and the bond angles deviate from 120 deg.

Figure 1(c) shows a representative atom A in the "unrolled" plane along with its three nearest-neighbor atoms B, C, and D. These four atoms A, B, C, and D characterize the positions of all atoms on the planar sheet in Fig. 1(b) since all atoms essentially result from the in-plane translation of these four atoms due to periodicity in the atomic structure of the CNT. Therefore, the lengths and angles between these four atoms completely characterize the planar structure in Fig. 1(b). Let $\mathbf{a}_1$ and $\mathbf{a}_2$ denote the vectors $\overrightarrow{BC}$ and $\overrightarrow{DC}$ in Fig. 1(c), respectively, and a_1 and a_2 be the corresponding lengths. The length of BD is denoted by a_3, and the lengths of AB and AC are denoted by a_4 and a_5, respectively (Fig. 1(c)). Other lengths and angles in the "unrolled" plane are completely determined by these five lengths a_i ($i=1,2,\ldots,5$). For example, two angles $\varphi_1=\angle CBD$ and $\varphi_2=\angle CBA$ (Fig. 1(c)), which will be used later to characterize the mapping between the CNT in Fig. 1(a) and the "unrolled" plane in Fig. 1(b), are given in terms of these five lengths a_i ($i=1,2,\ldots,5$) by

$$\varphi_1=\cos^{-1}\frac{a_1^2+a_3^2-a_2^2}{2a_1a_3},\quad \varphi_2=\cos^{-1}\frac{a_1^2+a_4^2-a_5^2}{2a_1a_4} \tag{1}$$

In order to characterize the actual atomic structure of the CNT shown in Fig. 1(a), it is necessary to prescribe the CNT diameter d_t and helicity which is represented by the angle θ between $\overrightarrow{BC}$ and the chiral vector $\mathbf{C}_h$ in Fig. 1(c), where $\mathbf{C}_h$ denotes the circumferential direction of the CNT in the planar sheet. It is pointed out that d_t and θ will be related to the charality of the CNT in the next paragraph. In the cylindrical coordinates (R,Θ,Z) of the CNT, the radial coordinates of all atoms are $R_A=R_B=R_C=R_D=d_t/2$. Without losing generality, we may take the polar angle and axial coordinate of atom B as zero, $\Theta_B=Z_B=0$. The axial coordinates of atoms A, C, and D equal to the projections of vectors $\overrightarrow{BA}$, $\overrightarrow{BC}$, and $\overrightarrow{BD}$ normal to the $\mathbf{C}_h$ direction (Fig. 1(c)), i.e.,

$$Z_A=a_4\sin(\varphi_2+\theta),\quad Z_C=a_1\sin\theta,\quad Z_D=a_3\sin(\varphi_1+\theta) \tag{2}$$

Similarly, the polar angles of atoms A, C, and D are related to the projections along the $\mathbf{C}_h$ direction (Fig. 1(c)), and are given by

$$\Theta_A=\frac{2a_4\cos(\varphi_2+\theta)}{d_t},\quad \Theta_C=\frac{2a_1\cos\theta}{d_t}$$

$$\Theta_D=\frac{2a_3\cos(\varphi_1+\theta)}{d_t} \tag{3}$$

The CNT diameter d_t and angle θ (Fig. 1) are related to the chirality (n,m) of the CNT. Following the standard notation for CNTs (e.g., [36]), the chiral vector $\mathbf{C}_h$, whose length equals the circumference of the CNT, can always be expressed in terms of the base vectors $\mathbf{a}_1$ and $\mathbf{a}_2$ as (Fig. 1(c))

$$\mathbf{C}_h=n\mathbf{a}_1+m\mathbf{a}_2 \tag{4}$$

where n and m are integers, $n\geq|m|\geq 0$, and the pair (n,m) is called the chirality of the CNT; $(n,0)$ and (n,n) are called the zigzag and armchair CNTs, respectively, while the general case $n>|m|>0$ is called the chiral CNT. Using the fact $\mathbf{a}_1\cdot\mathbf{a}_1=a_1^2$, $\mathbf{a}_2\cdot\mathbf{a}_2=a_2^2$, and $2\mathbf{a}_1\cdot\mathbf{a}_2=a_1^2+a_2^2-a_3^2$, we find the circumference of the CNT as

$$|\mathbf{C}_h|=\sqrt{\mathbf{C}_h\cdot\mathbf{C}_h}=\sqrt{n^2a_1^2+m^2a_2^2+nm(a_1^2+a_2^2-a_3^2)} \tag{5}$$

and the CNT diameter

$$d_t=\frac{|\mathbf{C}_h|}{\pi} \tag{6}$$

The angle θ is similarly obtained in terms of the chirality (n,m) as

$$\theta=\cos^{-1}\frac{\mathbf{C}_h\cdot\mathbf{a}_1}{|\mathbf{C}_h|a_1}=\cos^{-1}\frac{na_1^2+\frac{m}{2}(a_1^2+a_2^2-a_3^2)}{a_1|\mathbf{C}_h|} \tag{7}$$

Therefore, d_t and θ in Eqs. (6) and (7), as well as the spatial coordinates of atoms A, B, C, and D in Eqs. (2) and (3), are all given in terms of these five lengths a_i ($i=1,2,\ldots,5$).

2.2 Energy in the CNT. Since the positions of all atoms on the CNT are determined in terms of $a_1, a_2, \ldots, a_5$, the bond lengths and angles can also be obtained in terms of these five lengths. Here it is important to emphasize that the bond lengths and angles are for the bonds on the tubular structure of the CNT shown in Fig. 1(a) (instead of the "unrolled" planar sheet in Fig. 1(b)). For example, the bond length between two atoms X and Y ($X,Y=A,B,C,D$) with coordinates $(d_t/2,\Theta_X,Z_X)$ and $(d_t/2,\Theta_Y,Z_Y)$ is given by

$$r_{XY}^{(0)}=\sqrt{\frac{d_t^2}{2}[1-\cos(\Theta_Y-\Theta_X)]+(Z_Y-Z_X)^2} \tag{8}$$

which depends on these five lengths a_i ($i=1,2,\ldots,5$) for a given chirality (n,m) of the CNT.

Once all bond lengths and angles are known (in terms of these five lengths a_i ($i=1,2,\ldots,5$)), the energy stored in a bond can be obtained from the interatomic potential for carbon [33] given in the appendix. For example, the energy V_{AB} stored in the bond AB

Table 1 Bond lengths and angles in tubular configuration

	Chirality (n,m)	Diameter d_t (nm)	θ degree	Bond lengths (nm)			Bond angles (degree)		
				r_{AB}	r_{AC}	r_{AD}	$\angle BAC$	$\angle BAD$	$\angle CAD$
Graphite	$n+m\to\infty$	∞		0.14507	0.14507	0.14507	120	120	120
Zigzag	(30,0)	2.4021	0	0.14511	0.14511	0.14508	119.80	119.96	119.96
Nanotubes	(20,0)	1.6036	0	0.14516	0.14516	0.14510	119.55	119.92	119.92
	(10,0)	0.80771	0	0.14544	0.14544	0.14518	118.20	119.69	119.69
	(7,0)	0.57104	0	0.14586	0.14586	0.14528	116.28	119.40	119.40
	(5,0)	0.41522	0	0.14669	0.14669	0.14542	112.59	118.99	118.99
Armchair	(18,18)	2.4950	29.991	0.14509	0.14511	0.14509	119.87	120.02	119.87
Nanotubes	(12,12)	1.6646	29.979	0.14511	0.14517	0.14511	119.70	120.04	119.70
	(6,6)	0.83564	29.919	0.14525	0.14549	0.14525	118.80	120.17	118.80
	(5,5)	0.69797	29.887	0.14533	0.14568	0.14533	118.27	120.26	118.27
	(4,4)	0.56071	29.833	0.14548	0.14604	0.14548	117.31	120.45	117.31
Chiral	(25,9)	2.4425	14.786	0.14510	0.14511	0.14508	119.82	120.00	119.91
Nanotubes	(16,6)	1.5786	15.262	0.14514	0.14518	0.14510	119.57	120.01	119.79
	(9,3)	0.87112	13.794	0.14532	0.14544	0.14518	118.56	120.02	119.36
	(6,2)	0.58567	13.673	0.14564	0.14592	0.14531	116.72	120.07	118.61
	(4,2)	0.43355	18.702	0.14603	0.14675	0.14555	114.19	120.59	116.92

(Fig. 1) depends on the bond length r_{AB} and the angles between AB and neighbor bonds, i.e., $V_{AB}=V(r_{AB},\angle ABX)$, where X represents the neighbor atoms of A and B. The energy associated with the representative atom A is $1/2(V_{AB}+V_{AC}+V_{AD})$, which also depends on these five lengths a_i $(i=1,2,\ldots,5)$, where the factor 1/2 results from the equal split of the bond energy between the pair of atoms in each bond. The total potential energy in the CNT is $V_{\text{tot}}=N/2(V_{AB}+V_{AC}+V_{AD})$, where N is the total number of atoms on the CNT.

These five lengths a_i $(i=1,2,\ldots,5)$ are determined by minimizing the potential energy in the CNT in order to ensure the equilibrium, i.e.,

$$\frac{\partial}{\partial a_i}[V_{AB}+V_{AC}+V_{AD}]=0, \quad i=1,2,\ldots,5 \tag{9}$$

These are five nonlinear equations for a_i $(i=1,2,\ldots,5)$, and have to be solved numerically. Table 1 gives the numerical results of bond lengths, angles, CNT diameter, and orientation (angle θ) for several zigzag $[(n,0)]$, armchair $[(n,n)]$, and chiral $[(n,m),n>|m|>0]$ CNTs. The bond lengths and angles agree well with Sanchez–Portal et al.'s [37] ab initio atomistic studies for (4,4), (5,5), (6,6), (8,8), and (10,10) armchair CNTs based on the pseudopotential density functional theory. The results for a graphene sheet are also presented in Table 1 in order to show the effect of CNT diameter. It is observed that, for CNT diameters above 0.8 nm, the bond lengths and angles are essentially the same as those of graphene (within 1 percent difference) such that the CNT diameter has essentially no effect. However, for the smallest CNT diameter around 0.4 nm, the bond angle change is around 6 percent, which shows the significant effect of CNT diameter.

3 Coefficients of Thermal Expansion of Single Wall Carbon Nanotubes

3.1 Effect of Finite Temperature. The method described in section 2 to determine the bond lengths is only applicable at zero temperature. At a finite temperature, the total potential energy V_{tot} should be replaced by the Helmholtz free energy given by

$$A=V_{\text{tot}}-TS \tag{10}$$

where T is temperature, S is the entropy, $V_{\text{tot}}=N/2(V_{AB}+V_{AC}+V_{AD})$ is the total potential energy and it depends on these five lengths a_i $(i=1,2,\ldots,5)$. Based on the local harmonic model (e.g., [35,38]), the entropy is given by

$$S=-k_B\sum_{i=1}^{N}\sum_{\kappa=1}^{3}\ln\left[2\sinh\left(\frac{h\omega_{i\kappa}}{4\pi k_BT}\right)\right]$$
$$=-Nk_B\sum_{\kappa=1}^{3}\ln\left[2\sinh\left(\frac{h\omega_{\kappa}^{A}}{4\pi k_BT}\right)\right] \tag{11}$$

where N is the total number of atoms, k_B is the Boltzmann constant $1.38\times10^{-23}\,\text{J}\cdot\text{K}^{-1}$, h is the Planck's constant $6.63\times10^{-34}\,\text{J}\cdot\text{s}$, T is the temperature, and $\omega_{i\kappa}$ $(\kappa=1,2,3)$ are the vibration frequencies of atom i and are determined from the 3×3 local dynamic matrix $1/m_i\partial^2V_{\text{tot}}/\partial\mathbf{x}_i\partial\mathbf{x}_i$ of atom i by

$$\left|\omega_{i\kappa}^2\mathbf{I}-\frac{1}{m_i}\frac{\partial^2V_{\text{tot}}}{\partial\mathbf{x}_i\partial\mathbf{x}_i}\right|=0 \tag{12}$$

Here I is the 3×3 identity matrix, and m_i and $\mathbf{x}_i=(x_i,y_i,z_i)$ are the mass and Cartesian coordinates of atom i, respectively. For the CNT subject to temperature change, $\omega_{i\kappa}$ for the atom i are the same as those for the representation atom A, i.e., $\omega_{i\kappa}=\omega_{\kappa}^{A}$, where

$$\left|(\omega_{\kappa}^{A})^2\mathbf{I}-\frac{1}{m}\frac{\partial^2V_{\text{tot}}}{\partial\mathbf{x}^A\partial\mathbf{x}^A}\right|=0 \tag{13}$$

From (12) or (13), the vibration frequencies $\omega_{i\kappa}$ and ω_{κ}^{A} are also functions of these five lengths a_i $(i=1,2,\ldots,5)$. Therefore, the Helmholtz free energy A for the CNT also depends on a_i $(i=1,2,\ldots,5)$.

As discussed in section 2, these five lengths a_i $(i=1,2,\ldots,5)$ are determined by minimizing the potential energy in Eq. (9). But such an approach only holds at zero temperature. At a finite temperature T, atoms do not occupy static positions because of thermal vibrations. These five lengths a_i $(i=1,2,\ldots,5)$ now represent the average, ''equilibrium'' lengths at the finite temperature, and they are determined by minimizing the Helmholtz free energy (instead of the potential energy), i.e.,

$$\frac{\partial A[a_i(i=1,2,\ldots,5),T]}{\partial a_i}=0, \quad i=1,2,\ldots 5 \tag{14}$$

This gives these five lengths as a function of temperature, i.e., $a_i=a_i(T)$ $(i=1,2,\ldots,5)$.

3.2 Coefficients of Thermal Expansion. It is important to note that the temperature dependence of bond length at finite temperature results from the anharmonicity in the interatomic potential. For a strictly harmonic potential, the vibration frequencies $\omega_{i\kappa}$ are independent of atom positions such that the average, ''equilibrium'' bond lengths remain unchanged with the tempera-

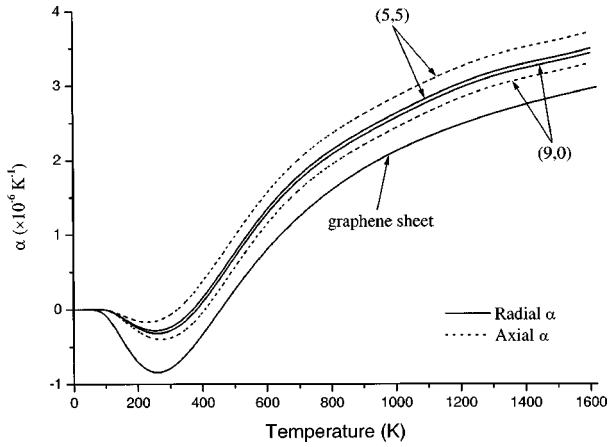

Fig. 2 The temperature dependence of the radial and axial coefficients of thermal expansion for (5,5) and (9,0) carbon nanotubes together with that for a flat graphene sheet

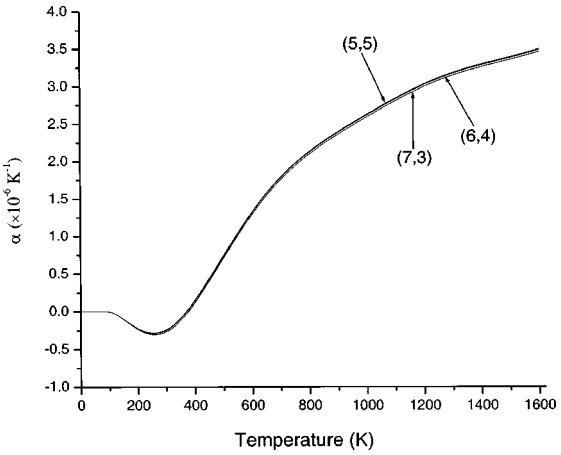

Fig. 3 The temperature dependence of the coefficient of thermal expansion in the radial direction for (5,5), (6,4), and (7,3) carbon nanotubes

ture increase, and therefore the CTEs vanish. This can be explained by the absolute isotropy in the tension/compression of atomic bonds characterized by the harmonic potential such that, even though the atoms vibrate, the center of vibration does not change with temperature. This is, however, not true for anharmonic potential such as Brenner's interatomic potential for carbon [33] which displays tension/compression anisotropy such that $\omega_{i\kappa}$ are not constants anymore, and the center of atom vibration changes with the temperature, leading to nonvanishing CTEs for CNTs.

The CNT diameter is related to these five lengths via Eqs. (5) and (6), and, therefore, also depends on the temperature T, $d_t = d_t(T)$. The CTE in the radial direction is given by

$$\alpha_{\text{radial}} = \frac{1}{d_t(T)} \frac{d[d_t(T)]}{dT} \tag{15}$$

The CTE in the axial direction can be similarly calculated from the variation of the translational vector which is the period in the axial direction (e.g., [36]). For example, the axial CTE for (n,n) armchair CNTs is determined from the change of BD (Fig. 1(c) and is given by

$$\alpha_{\text{axial}} = \frac{1}{a_3(T)} \frac{d[a_3(T)]}{dT}$$

For $(n,0)$ zigzag CNTs, the axial CTE is given by

$$\alpha_{\text{axial}} = \frac{1}{a_3(T)\sin\varphi_1(T)} \frac{d[a_3(T)\sin\varphi_1(T)]}{dT}$$

where the angle φ_1 is shown in Fig. 1(a) and is given in Eq. (1).

We use this method to study the radial and axial CTEs of single wall CNTs. Figure 2 shows the temperature dependence of radial and axial CTEs for a (5,5) armchair CNT and a flat graphene sheet. The CTEs are negative at low and room temperature, but become positive at high temperature for both the armchair CNT and the graphene sheet. This is, in fact, consistent with CTE data for graphite [34] which also show negative CTE at low and room temperature and positive CTE at high temperature. The molecular dynamic simulations of Raravikar et al. [31] did not report any temperature dependence of CTEs of CNTs, but they found that the radial CTE is less than the axial one for armchair CNTs, i.e., $\alpha_{\text{radial}} < \alpha_{\text{axial}}$. Our results for the (5,5) armchair CNT confirm this since the solid curve for radial CTE in Fig. 2 is below the dotted curve for axial CTE. However, for the (9,0) zigzag CNT, the opposite holds. Figure 2 also shows the temperature dependence of the radial and axial CTEs for the (9,0) zigzag CNT. The solid curve for the radial CTE of the (9,0) CNT is above the dotted curve for the axial CTE such that $\alpha_{\text{radial}} > \alpha_{\text{axial}}$. In fact, we have calculated the CTEs for other CNTs and found that $\alpha_{\text{radia}} < \alpha_{\text{axial}}$ for all armchair CNTs and $\alpha_{\text{radial}} > \alpha_{\text{axial}}$ for all zigzag CNTs. These CTEs are all negative at low and room temperature but become positive at high temperature.

We have chosen (5,5) and (9,0) CNTs in Fig. 2 because they have very close CNT diameters such that we can examine the effect of CNT helicity. It is observed that the axial CTEs curves are widely apart, but the radial CTEs curves are very close over the entire temperature range. The slight separation between two radial CTE curves may be due to the small difference in the diameters. We have also studied CNTs with almost identical diameters, such as (5,5), (6,4), and (7,3) CNTs. Their radial CTEs are shown in Fig. 3 and the curves are identical. This suggests that the radial CTE α_{radial} is independent of the CNT helicity, and depends only on the temperature and CNT diameter.

It is also observed from Figs. 2 and 3 that the CTE curves for (5,5) and (9,0) CNTs are above that for the graphene sheet. The ranges of negative CTE for CNTs become smaller due to the effect of finite CNT diameter. Figure 4 further shows the diameter-dependence of CTEs for armchair and zigzag CNTs at temperature $T = 400$ K. The armchair CNTs range from (5,5) to (11,11), while zigzag CNTs range from (9,0) to (20,0). The value of CTE of a graphene sheet is represented by the horizontal line. As the CNT diameter increases, the CTEs decrease and gradually approach that of the graphene sheet. At 400 K, the CTEs experience a change from positive to negative as the diameter increases.

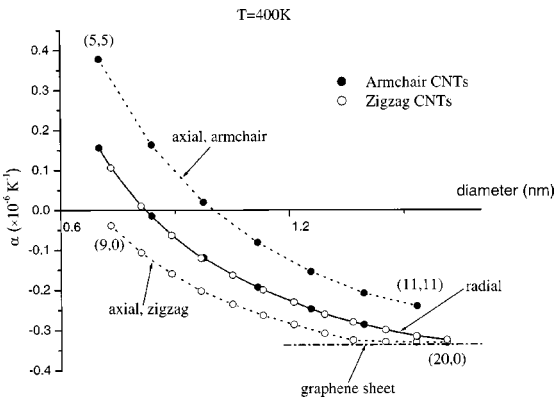

Fig. 4 The diameter-dependence of the coefficients of thermal expansion for armchair and zigzag carbon nanotubes at 400 K

Figure 4 also confirms that $\alpha_{\text{radial}} < \alpha_{\text{axial}}$ for armchair, $\alpha_{\text{radial}} > \alpha_{\text{axial}}$ for zigzag CNTs, and α_{radial} depends only on the CNT diameter.

4 Concluding Remarks

In conclusion, we have presented an analytic method to determine the coefficient of thermal expansion (CTE) for single wall carbon nanotubes based on the interatomic potential and the local harmonic model. The CTE in the radial direction of the CNT is less than that in the axial direction for armchair carbon nanotubes, but the opposite holds for zigzag carbon nanotubes. Furthermore, the CTE in the radial direction of the CNT is independent of the carbon nanotube helicity, while the axial CTE depends strongly on the helicity. The CTEs of carbon nanotubes are negative at low and room temperature but positive at high temperature. As the nanotube diameter decreases, the range of negative CTE shrinks.

Acknowledgment

Y.H. acknowledges insightful discussions with W. A. Curtin of Brown University, and the support from NSF (grants 00-99909, 01-03257, and the Nano CEMMS Center at UIUC), Office of Naval Research (grant N00014-01-1-0205, Program Manager Dr. Y. D. S. Rajapakse), Alexander von Humboldt Foundation, and NSFC. K.C.H. acknowledges support from NSFC and the Ministry of Education, China.

Appendix

The Empirical Bond Order Potential for Carbon. The interatomic potential for carbon [33] is given by

$$V(r_{ij};\theta_{ijk}) = V_R(r_{ij}) - \overline{B}_{ij} V_A(r_{ij}) \tag{A.1}$$

where r_{ij} is the distance between atoms i and j, θ_{ijk} represents the angle between the bond i-j and the neighbor bonds; and V_R and V_A are the repulsive and attractive pair terms given by

$$V_R(r) = \frac{D^{(e)}}{S-1} e^{-\sqrt{2S}\beta(r-R^{(e)})} f_c(r) \tag{A.2a}$$

$$V_A(r) = \frac{D^{(e)} S}{S-1} e^{-\sqrt{2/S}\beta(r-R^{(e)})} f_c(r) \tag{A.2b}$$

The parameters $D^{(e)}$, S, β, and $R^{(e)}$ are determined by fitting with known physical properties of various types of carbon. In particular, $R^{(e)}$ represents the equilibrium distance of two freestanding carbon atoms (i.e., no other atoms). The values of these parameters, as well as others introduced in Brenner's [33] interatomic potential, are given at the end of this section. The function f_c is merely a smooth cut-off function having the piecewise form

$$f_c(r) = \begin{cases} 1 & r < R^{(1)} \\ \frac{1}{2}\left\{1 + \cos\left[\frac{\pi(r-R^{(1)})}{R^{(2)}-R^{(1)}}\right]\right\} & R^{(1)} < r < R^{(2)} \\ 0 & r > R^{(2)} \end{cases} \tag{A.3}$$

where the effective range of the cut-off function is defined by $R^{(1)}$ and $R^{(2)}$.

The term $\overline{B}_{ij}$ in (A.1) represents a multi-body coupling term between the bond from atom i to atom j and the local environment of atom i. It reflects the contribution from other atoms in the local environment of atom i. This multi-body coupling term is given by

$$\overline{B}_{ij} = \frac{1}{2}(B_{ij} + B_{ji})$$
$$B_{ij} = \left[1 + \sum_{k(\neq i,j)} G(\theta_{ijk}) f_c(r_{ik})\right]^{-\delta} \tag{A.4}$$

where k denotes the carbon atoms other than i and j, r_{ik} is the distance between carbon atoms i and k, the exponent δ is given at the end of this section, f_c is the aforementioned cut-off function in (A.3), and θ_{ijk} defines the angle between carbon bonds i-j and i-k. The function G is given by

$$G(\theta) = a_0\left[1 + \frac{c_0^2}{d_0^2} - \frac{c_0^2}{d_0^2 + (1+\cos\theta)^2}\right] \tag{A.5}$$

where parameters a_0, c_0, and d_0, are determined by fitting to the known physical properties of various types of carbon.

Brenner [33] used the lattice constants and binding energies of graphite, diamond, simple cubic, and face-centered-cubic carbon, as well as vacancy formation energies of graphite and diamond to determine the parameters $D^{(e)}$, S, β, $R^{(1)}$, $R^{(2)}$, δ, a_0, c_0, and d_0 as

$$D^{(e)} = 6.000 \text{ eV}, \quad S = 1.22, \quad \beta = 21 \text{ nm}^{-1}$$
$$R^{(e)} = 0.1390 \text{ nm}$$
$$R^{(1)} = 0.17 \text{ nm}, \quad R^{(2)} = 0.20 \text{ nm}$$
$$\delta = 0.50000$$
$$a_0 = 0.00020813, \quad c_0 = 330, \quad d_0 = 3.5 \tag{A.6}$$

References

[1] Iijima, S., 1991, "Helical Microtubules of Graphite Carbon," Nature (London), **354**(6348), pp. 56–58.
[2] Ruoff, R. S., and Lorents, D. C., 1995, "Mechanical and Thermal Properties of Carbon Nanotubes," Carbon, **33**(7), pp. 925–930.
[3] Srivastava, D., Menon, M., and Cho, K. J., 2001, "Computational Nanotechnology With Carbon Nanotubes and Fullerenes," Comput. Sci. Eng., **3**(4), pp. 42–55.
[4] Yakobson, B. I., and Avouris, P., 2001, "Topics of Applied Physics," *Carbon Nanotubes*, M. S. Dresselhaus, G. Dresselhaus, and P. Avouris, **80**, pp. 287–329.
[5] Qian, D., Wagner, G. J., Liu, W. K., Yu, M.-F., and Ruoff, R. S., 2002, "Mechanics of Carbon Nanotubes," Appl. Mech. Rev., **55**(6), pp. 495–553.
[6] Thostenson, E. T., Ren, Z., and Chou, T. W., 2001, "Advances in the Science and Technology of Carbon Nanotubes and Their Composites: A Review," Combust. Sci. Technol., **61**(13), pp. 1899–1912.
[7] Heath, J. R., 2002, "Wires, Switches, and Wiring: A Route Toward a Chemically Assembled Electronic Nanocomputer," Pure Appl. Chem., **72**(1–2), pp. 11–20.
[8] Tans, S. J., Verschueren, A. R. M., and Dekker, C., 1998, "Room-Temperature Transistor Based on a Single Carbon Nanotube," Nature (London), **393**(6680), pp. 49–52.
[9] Hu, J. T., Min, O. Y., Yang, P. D., and Lieber, C. M., 1999, "Controlled Growth and Electrical Properties of Heterojunctions of Carbon Nanotubes and Silicon Nanowires," Nature (London), **399**(6731), pp. 48–49.
[10] Bachtold, A., Hadley, P., Nakanishi, T., and Dekker, C., 2001, "Logic Circuits With Carbon Nanotube Transistors," Science, **294**(5545), pp. 1317–1320.
[11] Appenzeller, J., Knoch, J., Derycke, V., Martel, R., Wind, S., and Avouris, P., 2002, "Field-Modulated Carrier Transport in Carbon Nanotube Transistors," Phys. Rev. Lett., **89**(12), pp. 126801-1–120801-4.
[12] Avouris, P., Martel, R., Derycke, V., and Appenzeller, J., 2002, "Carbon Nanotube Transistors and Logic Circuits," Physica B, **323**(1–4), pp. 6–14.
[13] Derycke, V., Martel, R., Appenzeller, J., and Avouris, P., 2002, "Controlling Doping and Carrier Injection in Carbon Nanotube Transistors," Appl. Phys. Lett., **80**(15), pp. 2773–2775.
[14] Leonard, F., and Tersoff, J., 2002, "Multiple Functionality in Nanotube Transistors," Appl. Phys. Lett., **88**(25), pp. 258302-1–258302-4.
[15] Rosenblatt, S., Yaish, Y., Park, J., Gore, J., Sazonova, V., and McEuen, P. L., 2002, "High Performance Electrolyte Gated Carbon Nanotube Transistors," Nano Lett., **2**(8), pp. 869–872.
[16] Swenson, C. A., 1983, "Recommended Values for the Thermal Expansivity of Silicon From 0-K to 1000-K," J. Phys. Chem. Ref. Data, **12**(2), pp. 179–182.
[17] Kagaya, H. M., and Soma, T., 1985, "Temperature-Dependence of the Linear Thermal-Expansion Coefficient for Si and Ge," Phys. Status Solidi B, **129**(1), pp. K5–K8.

[18] White, G. K., and Minges, M. L., 1985, *Thermophysical Properties of Some Key Solids*, Pergamon, New York.
[19] Kayago, H. M., Shoji, N., and Soma, T., 1987, ''Specific-Heat and Thermal-Expansion at High-Temperatures of Si and Ge,'' Phys. Status Solidi B, **142**(1), pp. K13–K17.
[20] Madelung, O., 1987, *Landolt-Bornstein, New Series, Intrinsic Properties of Group IV Elements and III–V, II–VI, and I–VII Compounds*, Springer-Verlag, Berlin.
[21] Biernacki, S., and Scheffler, M., 1989, ''Negative Thermal Expansion of Diamond and Zinc-Blende Semiconductors,'' Phys. Rev. Lett., **63**(3), pp. 290–293.
[22] Buda, F., Car, R., and Parrinello, M., 1990, ''Thermal-Expansion of C-Si Via Ab Initio Molecular-Dynamics,'' Phys. Rev. B, **41**(3), pp. 1680–1683.
[23] Xu, C. H., Wang, C. Z., Chan, C. T., and Ho, K. M., 1991, ''Theory of the Thermal Expansion of Si and Diamond,'' Phys. Rev. B, **43**(6), pp. 5024–5027.
[24] Biernacki, S., and Scheffler, M., 1994, ''The Influence of the Isotopic Composition on Crystalline Si,'' J. Phys.: Condens. Matter, **6**(26), pp. 4879–4884.
[25] Fabian, J., and Allen, P. B., 1997, ''Thermal Expansion and Gruneisen Parameters of Amorphous Silicon: A Realistic Model Calculation,'' Phys. Rev. Lett., **79**(10), pp. 1885–1888.
[26] Bandow, S., 1997, ''Radial Thermal Expansion of Purified Multiwall Carbon Nanotubes Measured by X-Ray Diffraction,'' Jpn. J. Appl. Phys., Part 2, **36**(10B), pp. 1403–1405.
[27] Maniwa, Y., Fujiwara, R., Kira, H., Tou, H., Nishibori, E., Takata, M., Sakata, M., Fujiwara, A., Zhao, X., Jijima, S., and Ando, Y., 2001, ''Multiwalled Carbon Nanotubes Grown in Hydrogen Atmosphere: A X-Ray Diffractionf Study,'' Phys. Rev. B, **64**(7), pp. 073105-1–073105-4.
[28] Yosida, Y., 2000, ''High-Temperature Shrinkage of Single-Walled Carbon Nanotube Bundles up to 1600K,'' J. Appl. Phys., **87**(7), pp. 3338–3341.
[29] Maniwa, Y., Fujiwara, R., Kira, H., Tou, H., Kataura, H., Suzuki, S., Achiba, Y., Nishibori, E., Takata, M., Sakata, M., Fujiwara, A., and Suematsu, H., 2001, ''Thermal Expansion of Single-Walled Carbon Nanotube (SWNT) Bundles: X-Ray Diffraction Studies,'' Phys. Rev. B, **64**(24), pp. 241402-1–241402-3.
[30] Wei, C., Srivastava, D., and Cho, K., 2002, ''Thermal Expansion and Diffusion Coefficients of Carbon Nanotube-Polymer Composites,'' Nano Lett., **2**(6), pp. 647–650.
[31] Raravikar, N. R., Keblinski, P., Rao, A. M., Dresselhaus, M. S., Schadler, L. S., and Ajayan, P. M., 2002, ''Temperature Dependence of Radial Breathing Mode Raman Frequency of Single-Walled Carbon Nanotubes,'' Phys. Rev. B, **66**(23), pp. 235424-1–235424-9.
[32] Tersoff, J., 1988, ''New Empirical Approach for the Structure and Energy of Covalent Systems,'' Phys. Rev. B, **37**(12), pp. 6991–7000.
[33] Brenner, D. W., 1990, ''Empirical Potential for Hydrocarbons for Use in Simulating the Chemical Vapor Deposition of Diamond Films,'' Phys. Rev. B, **42**(15), pp. 9458–9471.
[34] Billings, B. H., and Gray, D. E., 1972, *American Institute of Physics Handbook*, McGraw-Hill, New York.
[35] Chandler, D., 1987, *Introduction to Modern Statistical Mechanics*, Oxford University Press, Oxford.
[36] Saito, R., Dresselhaus, G., and Dresselhaus, M. S., 1998, *Physical Properties of Carbon Nanotubes*, Imperial College Press, London.
[37] Sanchez-Portal, D., Artacho, E., and Solar, J. M., 1999, ''Ab Initio Structure, Elastic, and Vibrational Properties of Carbon Nanotubes,'' Phys. Rev. B, **59**(19), pp. 12678–12688.
[38] Foiles, S. M., 1994, ''Evaluation of Harmonic Methods for Calculating the Free Energy of Defects in Solids,'' Phys. Rev. B, **49**(21), pp. 14930–14938.